

# Photoelectron spectroscopy of aromatic compound clusters of the B<sub>12</sub> all-boron benzene: B<sub>12</sub>Au<sup>−</sup> and B<sub>12</sub>(BO)<sup>−</sup>†

Cite this: *Phys. Chem. Chem. Phys.*, 2013, **15**, 9646

Hui Bai,<sup>a</sup> Hua-Jin Zhai,<sup>ab</sup> Si-Dian Li<sup>\*a</sup> and Lai-Sheng Wang<sup>\*b</sup>

We report a photoelectron spectroscopy and density-functional theory study of the B<sub>12</sub>Au<sup>−</sup> and B<sub>13</sub>O<sup>−</sup> clusters and their neutrals, which are shown to be six  $\pi$  electron aromatic compounds between the quasi-planar all-boron B<sub>12</sub> benzene-analogue and a monovalent Au or BO ligand. Electron affinities of B<sub>12</sub>Au and B<sub>13</sub>O are measured to be  $3.48 \pm 0.04$  and  $3.90 \pm 0.04$  eV, respectively. Structural searches are performed for B<sub>12</sub>Au<sup>−</sup> and B<sub>13</sub>O<sup>−</sup>, which are compared with the isovalent B<sub>12</sub>H<sup>−</sup> cluster. The global minima of B<sub>12</sub>Au<sup>−</sup> and B<sub>13</sub>O<sup>−</sup> both feature an almost intact B<sub>12</sub> cluster with the Au and BO ligands bonded to its periphery, respectively. For B<sub>12</sub>Au<sup>−</sup>, a low-lying isomer is also identified, which is only 0.4 kcal mol<sup>−1</sup> above the global minimum, in agreement with the experimental observation of a weakly populated isomer in the cluster beam of B<sub>12</sub>Au<sup>−</sup>. These aromatic compound clusters provide new examples for the Au/H isolobal analogy and the boronyl (BO) chemistry.

Received 14th January 2013,

Accepted 17th April 2013

DOI: 10.1039/c3cp50167a

[www.rsc.org/pccp](http://www.rsc.org/pccp)

## 1. Introduction

In contrast to bulk boron where three-dimensional B<sub>12</sub> cage units dominate, elemental boron clusters exhibit planar or quasi-planar structures up to very large sizes<sup>1–14</sup> that are unparalleled in any other elements in the periodic table. The critical size for two-dimensional (2D) to three-dimensional (3D) transition is established to be B<sub>16</sub><sup>+</sup> for cations,<sup>13</sup> B<sub>20</sub> for neutrals,<sup>10</sup> and beyond B<sub>23</sub><sup>−</sup> for anionic clusters,<sup>6–11</sup> for which the exact size for 2D-to-3D transition is yet to be determined. Among all boron clusters characterized so far, the B<sub>12</sub> neutral shows unique electronic and structural properties.<sup>6</sup> As revealed from the B<sub>12</sub><sup>−</sup> anion photoelectron spectra, the B<sub>12</sub> cluster possesses a 2.0 eV energy gap between its highest occupied molecular orbital (HOMO) and lowest unoccupied molecular

orbital (LUMO), the greatest of all B<sub>n</sub> ( $n = 3–23$ ) clusters.<sup>6–11</sup> Both B<sub>12</sub> and B<sub>12</sub><sup>−</sup> adopt quasi-planar structures with a circular shape,<sup>6</sup> as does their cationic counterpart, B<sub>12</sub><sup>+</sup>.<sup>13</sup> Bonding analysis shows that B<sub>12</sub> is an aromatic system with six  $\pi$  electrons and may be considered as a prototypical all-boron benzene, similar to the “magic” B<sub>13</sub><sup>+</sup> cluster in prior mass spectrometric studies.<sup>3,4,14</sup> Computational “design” of a fluxional B<sub>9</sub>C<sub>3</sub><sup>3+</sup> molecular wheel,<sup>15</sup> which is isoelectronic to B<sub>12</sub>, was also reported, albeit such B<sub>9</sub>C<sub>3</sub><sup>3+</sup> wheel is not the global minimum structure. The quasi-planarity of B<sub>12</sub> was recently found to be entirely due to a “mechanical” effect to fit three boron atoms in a B<sub>9</sub> ring, as revealed from isoelectronic substitution by Al in B<sub>11</sub>Al.<sup>16</sup>

Compound clusters based on B<sub>12</sub>, in particular its hydrogenation, have also been actively pursued lately.<sup>17–22</sup> A primary motivation of these studies was to address the planar to cage structural transition in B<sub>12</sub>H<sub>n</sub> as a function of hydrogen content, as the dodecaborane dianion B<sub>12</sub>H<sub>12</sub><sup>2−</sup> is known to be a stable icosahedral cage. A planar D<sub>3h</sub> borozene molecule B<sub>12</sub>H<sub>6</sub> was proposed initially,<sup>17</sup> and its potential as a building block for large aromatic compounds explored.<sup>18</sup> Subsequent systematic computational data on B<sub>12</sub>H<sub>n</sub> ( $n = 1–8$ ) showed, however, that the proposed borozene B<sub>12</sub>H<sub>6</sub> structure is not the global minimum and instead a cage-like structure was found to be substantially lower in energy by 35 kcal mol<sup>−1</sup> at the CCSD(T) level.<sup>20</sup> Computational data also revealed that in B<sub>12</sub>H<sub>n</sub> and B<sub>12</sub>H<sub>n</sub><sup>−</sup> clusters the cage-like structures gradually gain stability relative to the planar ones with increasing  $n$ , and a planar-to-cage structural transition

<sup>a</sup> Institute of Molecular Science, Shanxi University, Taiyuan 030006, P. R. China.  
E-mail: [lisidian@sxu.edu.cn](mailto:lisidian@sxu.edu.cn)

<sup>b</sup> Department of Chemistry, Brown University, Providence, Rhode Island 02912, USA. E-mail: [Lai-Sheng\\_Wang@brown.edu](mailto:Lai-Sheng_Wang@brown.edu)

† Electronic supplementary information (ESI) available: Alternative optimized structures for B<sub>12</sub>Au<sup>−</sup>, B<sub>13</sub>O<sup>−</sup>, and B<sub>12</sub>H<sup>−</sup>, and selected neutral structures at B3LYP level (Fig. S1–S3); comparisons of the potential energy surfaces of B<sub>12</sub>H<sup>−</sup>, B<sub>12</sub>Au<sup>−</sup>, and B<sub>13</sub>O<sup>−</sup> (Fig. S4) and their simulated photoelectron spectra (Fig. S5); molecular orbitals for the global minimum structures of B<sub>12</sub><sup>−</sup>, B<sub>12</sub>H<sup>−</sup>, B<sub>12</sub>Au<sup>−</sup>, and B<sub>13</sub>O<sup>−</sup> (Fig. S6–S8) and their analysis (Table S1); calculated vibrational frequencies of B<sub>12</sub>Au, B<sub>13</sub>O, and B<sub>12</sub>H neutral clusters at B3LYP level (Table S2); and Cartesian coordinates and total energies for selected anion and neutral cluster structures at the B3LYP level (Table S3). See DOI: 10.1039/c3cp50167a

occurs at around  $n = 4$ .<sup>19–21</sup> Experimentally,  $B_{12}H_n^+$  clusters were generated in ion–molecule reactions in an ion trap, revealing  $B_{12}H_8^+$  as the most abundant species. However, spectroscopic characterizations of these hydride clusters were not possible due to isotopic mass mixing.<sup>22</sup>

In the current work, we investigate the  $B_{12}Au^-$  and  $B_{13}O^-$  clusters and their neutral species. These clusters turn out to be aromatic compounds between the quasi-planar  $B_{12}$  cluster and a monovalent Au and BO ligand, respectively, which are isovalent to the  $B_{12}H^-$  and  $B_{12}H$  clusters. The current results extend the Au/H isolobal analogy<sup>23–26</sup> and the boron boronyl chemistry.<sup>27–30</sup> The structural and bonding analogy between a bare gold atom and H was discovered in gas-phase binary Au clusters, such as Si–Au clusters, where  $SiAu_4$ ,  $SiAu_n$  ( $n = 2, 3$ ),  $Si_2Au_n$  ( $n = 2, 4$ ), and  $Si_3Au_3$  were demonstrated to possess structures and bonding similar to the  $SiH_4$  silane,  $SiH_n$ ,  $Si_2H_n$ , and  $Si_3H_3$ , respectively.<sup>24</sup> A subsequent study<sup>23</sup> showed that the B–Au bonding in  $B_7Au_2^-$  cluster is highly covalent and similar to the B–H bonding in the  $B_7H_2^-$  cluster.<sup>31</sup> The  $B_{10}Au^-$  cluster<sup>30</sup> served as another example of the Au/H analogy in Au-doped boron clusters. The concept of Au/H analogy has also been used to consider the viability of deltahedral *closo*-auro-boranes species,  $B_nAu_n^{2-}$ , analogous to the spherically aromatic *closo*-boranes  $B_nH_n^{2-}$  ( $n = 5–12$ ).<sup>26</sup> While working on boron oxide clusters,<sup>27–30</sup> we discovered lately that the boronyl (BO) group governs the structure and bonding in the boron-rich oxide systems. We characterized a number of these clusters, such as  $B_3O_2^-$ ,  $B_4O_3^-$ , and  $B_5O_4^-$ , which possess linear, triangular, and tetrahedral global minimum structures with terminal BO groups, respectively.<sup>28,30</sup> We also studied the  $B_4O_2^{2-}$  cluster with a rare  $B \equiv B$  triple bond.<sup>29</sup> Furthermore, we characterized the bridging  $\eta^2$ -BO groups in  $B_2(BO)_3^-$  and  $B_3(BO)_3^-$  clusters.<sup>30</sup> The boronyl group can thus act as either a terminal or bridging ligand and is capable of forming the three-center two-electron (3c-2e) bridging bonds, showing isolobal analogy between boron-rich oxide clusters and boranes. Boron oxide clusters are also the topic of numerous recent computational studies.<sup>32,33</sup> The first isolable metal boronyl compound,<sup>34</sup> and the first complex with a  $B \equiv B$  triple bond as well,<sup>35</sup> were lately synthesized in the bulk.

Here we report a combined photoelectron spectroscopy (PES) and density-functional theory (DFT) study on the  $B_{12}Au^-$  and  $B_{13}O^-$  clusters. The potential energy surfaces of  $B_{12}Au^-$ ,  $B_{13}O^-$ , and  $B_{12}H^-$  are shown to be similar to each other. The Au and BO ligands modify only very slightly the electronic properties of  $B_{12}Au^-$  and  $B_{13}O^-$  clusters relative to those of  $B_{12}^-$  and  $B_{12}H^-$ . The aromaticity due to the six  $\pi$  electrons in  $B_{12}$  remains intact in the Au and BO compounds.

## 2. Experimental and theoretical methods

### 2.1. Photoelectron spectroscopy

The experiment was carried out using a magnetic-bottle-type PES apparatus equipped with a laser vaporization supersonic cluster source, the details of which were described elsewhere.<sup>36</sup> Briefly, the  $B_{12}Au^-$  cluster anions were produced by laser vaporization of an Au/B mixed disk target (99.75%  $^{10}B$  enriched), in

the presence of a pure helium carrier gas, whereas the  $B_{13}O^-$  clusters were produced using a boron disk target made of  $^{10}B$ -enriched isotope (99.75%) in the presence of a helium carrier gas seeded with 0.01%  $O_2$ . The cluster anions were analyzed using a time-of-flight mass spectrometer, and the  $B_{12}Au^-$  and  $B_{13}O^-$  clusters of interest were each mass-selected and decelerated before being photodetached. Due to the relatively high electron binding energies of these species, two detachment photon energies were used in the current experiment: 266 nm (4.661 eV) from a Nd:YAG laser and 193 nm (6.424 eV) from an ArF excimer laser. Effort was made to choose colder clusters (that is, those with long resident times in the nozzle) for photodetachment, which was shown previously to be critical for obtaining high quality PES data.<sup>37</sup> Photoelectrons were collected at nearly 100% efficiency by the magnetic bottle and analyzed in a 3.5 m long electron flight tube. The PES spectra were calibrated using the known spectra of  $Rh^-$  and  $Au^-$ . The energy resolution of the apparatus was  $\Delta E_k/E_k \approx 2.5\%$ , that is,  $\sim 25$  meV for 1 eV kinetic energy electrons.

### 2.2. Computational methods

Structural searches for  $B_{12}Au^-$  and  $B_{13}O^-$  were performed initially at the hybrid B3LYP level<sup>38</sup> with the 3-21G basis set,<sup>39</sup> using the Coalescence Kick (CK) global minimum search program.<sup>8,40</sup> The top 12 low-lying candidate structures were then fully optimized at the B3LYP level with the 6-311G(d,p) basis set<sup>41</sup> for B, O, and H and the Stuttgart relativistic small-core pseudopotential and valence basis set augmented with two *f* and one *g* functions for Au [ $\alpha(f) = 0.498, 1.461$ ;  $\alpha(g) = 1.218$ ],<sup>42</sup> denoted hereafter as Stuttgart\_rsc\_1997\_ecp+2f1g. Relevant low-lying neutral structures were also optimized. For the purpose of comparison, the same set of structures was also calculated for  $B_{12}H^-$  and  $B_{12}H$ . Frequency calculations were done to confirm that the obtained structures are true minima, unless stated otherwise. Excitation energies of the neutral clusters were calculated with the time-dependent DFT (TD-DFT) method<sup>43</sup> at the ground-state structures of the anions. Additional single-point CCSD(T)<sup>44</sup> calculations were done at the B3LYP/B<sub>3</sub>O<sub>3</sub>H/6-311G(d,p)/Au/Stuttgart\_rsc\_1997\_ecp+2f1g geometries to further evaluate the relative energies of the top four low-lying anion structures and to refine the ground-state adiabatic and vertical detachment energies (ADEs and VDEs). All calculations were carried out using the Gaussian 03 package.<sup>45</sup>

## 3. Experimental results

### 3.1. $B_{12}Au^-$

The PES spectra of  $B_{12}Au^-$  are shown in Fig. 1 at two detachment energies. The 266 nm spectrum reveals two intense bands (X and A; Fig. 1a) and two additional weak features in between. The ground-state band X is relatively broad with a VDE of 3.59 eV (Table 1), as measured from the band maximum. Since no vibrational structures are resolved for band X, the ADE is estimated by drawing a straight line along the well-defined leading edge of band X and then adding the instrumental resolution to the intersection with the binding energy axis.

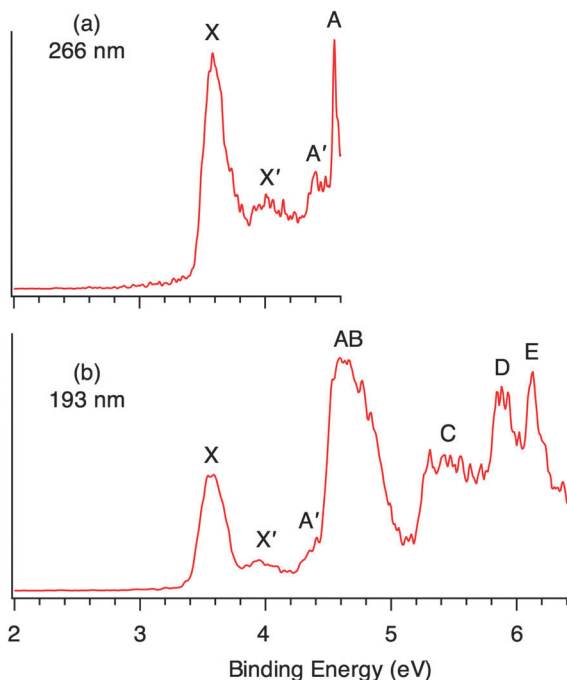


**Fig. 1** Photoelectron spectra of  $B_{12}Au^-$  at (a) 266 nm (4.661 eV) and (b) 193 nm (6.424 eV).

**Table 1** Experimental adiabatic and vertical detachment energies (ADEs and VDEs; in eV) from the photoelectron spectra of  $B_{12}Au^-$ , as compared with theoretical calculations based on the global minimum (1) and low-lying structures (2 and 3) at the B3LYP/B-6-311G(d,p)/Au/Stuttgart\_rsc\_1997\_ecp+2f1g and TD-DFT levels

Feature	ADE (expt)	VDE (expt)	VDE (1)	VDE (2)	VDE (3)
X	$3.48 \pm 0.04^a$	$3.59 \pm 0.02$	3.34 (3.40) <sup>b,c</sup>		3.57 (3.66) <sup>c</sup>
X'		$\sim 4.0^d$		3.76 (3.85) <sup>c</sup>	
A'		$\sim 4.4^d$		4.27	4.42
A	$4.55 \pm 0.01$	4.51	4.51	4.51	4.44
B	$4.64 \pm 0.05^e$	4.67			
C	$\sim 5.5^e$	5.19	5.11	5.05	
		5.35	5.51	5.21	
D	$5.89 \pm 0.03$	5.76	5.82	5.76	
E	$6.12 \pm 0.02$	5.96	6.08		

<sup>a</sup> Electron affinity of the neutral cluster. <sup>b</sup> Numbers in *italic* in the parentheses are from the single-point CCSD(T)/B3LYP/B-6-311G(d,p)/Au/Stuttgart\_rsc\_1997\_ecp+2f1g calculations. <sup>c</sup> Calculated ADEs are 3.16 (3.24), 3.56 (3.59), and 3.46 (3.52) eV for structures 1, 2, and 3, respectively. <sup>d</sup> From minor isomer. <sup>e</sup> Center of the overlapping transitions.

The ADE thus obtained is  $3.48 \pm 0.04$  eV, which is also the electron affinity of  $B_{12}Au$  neutral. Band A at 4.55 eV is sharp, being separated from band X by a  $\sim 1.0$  eV energy gap. Continuous weak signals, which are attributed to a minor isomer, are present in between bands X and A. Two bands are tentatively labeled: X' ( $\sim 4.0$  eV) and A' ( $\sim 4.4$  eV).

The 193 nm spectrum reveals numerous higher binding energy bands (Fig. 1b). Band B appears to be overlapping with band A, resulting in an intense and broad peak. The center of A/B peak (4.64 eV) should be viewed as the average of two VDEs. Beyond bands A/B, a broad band C ( $\sim 5.5$  eV) roughly covers the

energy range from 5.2 to 5.7 eV and likely contains overlapping electronic transitions, as well. At higher binding energies, two relatively sharp bands are observed: D (5.89 eV) and E (6.12 eV).

### 3.2. $B_{13}O^-$

The 266 nm PES spectrum of  $B_{13}O^-$  (Fig. 2a) shows a broad band X for the ground-state transition with an ADE and VDE of  $3.90 \pm 0.04$  and 4.04 eV, respectively (Table 2). The ADE also represents the electron affinity of  $B_{13}O$  neutral. Following an energy gap of  $\sim 0.8$  eV, four well-defined excited-state bands (A, B, C, and D; Fig. 2b) are observed in the 193 nm spectrum at VDEs of 4.84, 5.32, 5.74, and 6.15 eV, respectively. The relatively clean and well-resolved PES bands for  $B_{13}O^-$  suggest that there is only one isomer present in the cluster beam.

## 4. Computational results

All cluster structures presented herein are at the B3LYP/B<sub>3</sub>O<sub>2</sub>H/6-311G(d,p)/Au/Stuttgart\_rsc\_1997\_ecp+2f1g level of theory. The global minima and two low-lying structures of  $B_{12}Au^-$  (1–3),  $B_{12}Au$  (13–15),  $B_{13}O^-$  (16–18), and  $B_{13}O$  (28–30) are depicted in Fig. 3. Alternative optimized structures are summarized in Fig. S1 and S2 in the ESI† for  $B_{12}Au^-$  (1–12) and  $B_{13}O^-$  (16–27) anion clusters, as well as their relevant  $B_{12}Au$  (13–15) and  $B_{13}O$  (28–30) neutral clusters. To aid the analysis of chemical bonding, a similar set of structures is also optimized for  $B_{12}H^-$  (31–42) and  $B_{12}H$  (43–46) (Fig. S3 in ESI†). Nearly all these structures are true minima on their potential energy surfaces, except for structures 14, 26, and 40 which correspond to first or second order saddle points.

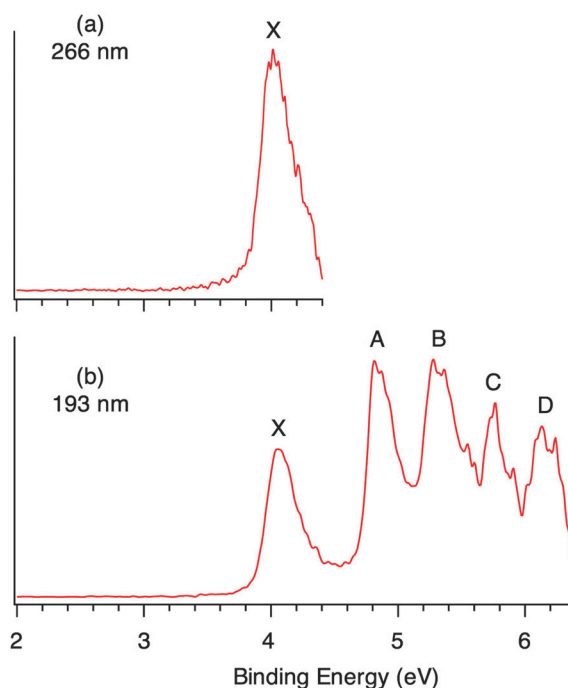


**Fig. 2** Photoelectron spectra of  $B_{13}O^-$  at (a) 266 nm and (b) 193 nm.

**Table 2** Experimental adiabatic and vertical detachment energies (ADEs and VDEs; in eV) from the photoelectron spectra of  $B_{13}O^-$ , as compared with theoretical calculations based on the global minimum (**16**) and low-lying structures (**17** and **18**) at the B3LYP/6-311G(d,p) and TD-DFT levels

Feature	ADE (expt)	VDE (expt)	VDE ( <b>16</b> )	VDE ( <b>17</b> )	VDE ( <b>18</b> )
X	$3.90 \pm 0.04^a$	$4.04 \pm 0.03$	3.76 (3.81) <sup>b,c</sup>	3.86 (3.94) <sup>c</sup>	
A		$4.84 \pm 0.03$	4.77	4.58 (4.49) <sup>c</sup>	4.65
B		$5.32 \pm 0.05$	5.14	4.78	5.16
C		$5.74 \pm 0.03$	5.40	5.32	5.61
D		$6.15 \pm 0.05$	5.92	6.12	5.96

<sup>a</sup> Electron affinity of the neutral cluster. <sup>b</sup> Numbers in *italic* in the parentheses are from the single-point CCSD(T)//B3LYP/6-311G(d,p) calculations. <sup>c</sup> Calculated ADEs are 3.56 (3.66), 4.20 (4.26), and 3.72 (3.76) eV for structures **16**, **17**, and **18**, respectively.

#### 4.1. $B_{12}Au^-$ and $B_{12}Au$

The top three low-lying structures of  $B_{12}Au^-$  (**1–3**) (Fig. 3) and an additional higher-energy structure **5** (Fig. S1 in ESI†) are based on the global minimum of the  $B_{12}$  cluster with the Au atom bonded either to the outer  $B_9$  or inner  $B_3$  rings. Structure **1** ( $C_1$ ,  $^1A$ ) is the global minimum. However, structures **2** ( $C_s$ ,  $^1A'$ ) and **3** ( $C_s$ ,  $^1A'$ ) are competitive, which are within  $\sim 0.5$  kcal mol $^{-1}$  above the  $C_1$  global-minimum structure at the single-point CCSD(T)//B3LYP/B/6-311G(d,p)/Au/Stuttgart\_rsc\_1997\_ecp+2f1g level. All other anion structures as shown in Fig. S1 in the ESI† are considerably higher in energy.

Selected structures of  $B_{12}Au$  neutral cluster, corresponding to the top three anionic structures, are optimized (**13–15**; Fig. 1). Structure **13** is the lowest in energy and closely resembles the anionic global-minimum structure **1**. Note that structures **14** and **15**, which correspond to the low-lying anionic isomers **2** and **3**, are located more than 10 kcal mol $^{-1}$  above **13**.

#### 4.2. $B_{13}O^-$ and $B_{13}O$

It is clear that all  $B_{13}O^-$  structures, of which the top three low-lying structures (**16–18**) are shown in Fig. 3 and higher energy structures (**19–27**) collected in Fig. S2 in the ESI† are not related to the bare  $B_{13}^-$  cluster.<sup>6</sup> Instead, the boronyl BO unit is featured in all the  $B_{13}O^-$  structures. The global minimum **16** ( $C_1$ ,  $^1A$ ) is based on the global minimum of  $B_{12}$  with a BO group bonded to an apex of the outer ring, closely resembling the global minimum of  $B_{12}Au^-$  (**1**). The next lowest energy structure **17** ( $C_s$ ,  $^1A'$ ) of  $B_{13}O^-$  also resembles that of  $B_{12}Au^-$  (**2**). The third lowest energy structure **18** ( $C_1$ ,  $^1A$ ) of  $B_{13}O^-$  possesses a distorted  $B_{12}$  motif, which includes a planar hepta-coordinate boron center.<sup>7</sup> Structures **17** and **18** are  $\sim 3$  kcal mol $^{-1}$  above the global minimum at the single-point CCSD(T)//B3LYP/6-311G(d,p) level. Note that owing to intramolecular coulomb repulsion, BO bonding to the  $B_{12}$  core appears to favor the low-coordinate apex sites as compared to the on-top site (Fig. S2 in ESI†), akin to CO chemisorption on nanogold.<sup>46</sup> This makes the  $B_{13}O^-$  cluster structurally more selective, as shown in Fig. S4 in the ESI†. Alternative optimized structures **19–27** of  $B_{13}O^-$  are 7–48 kcal mol $^{-1}$  higher in energy, where structure **19** corresponds to the low-lying structure **3** of  $B_{12}Au^-$ .

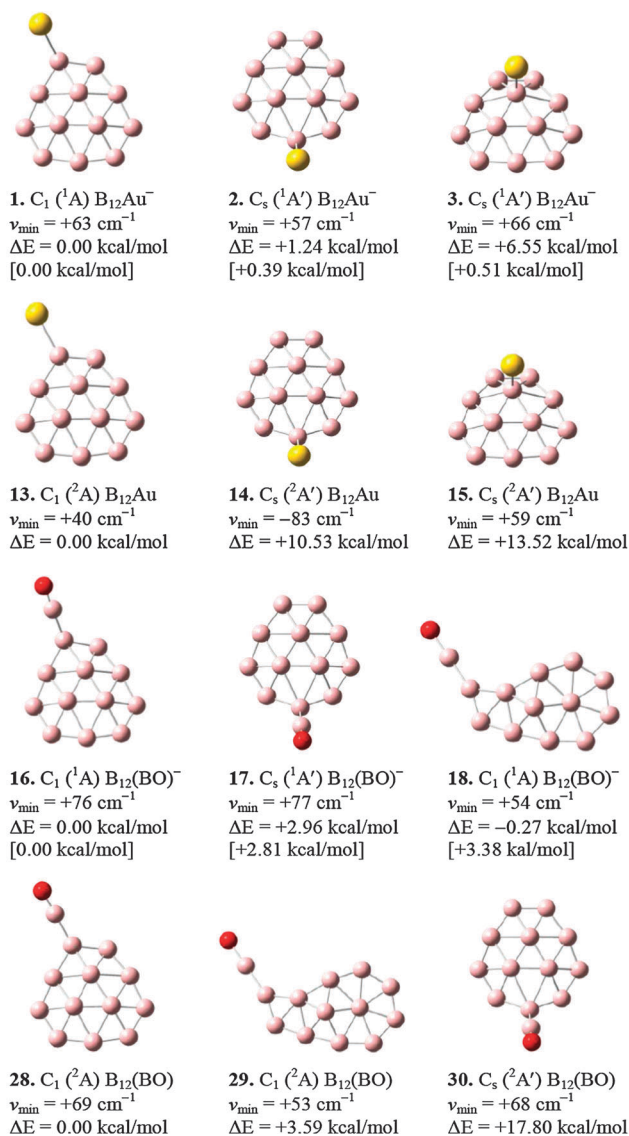


**Fig. 3** Optimized anion global-minimum structures (**1** for  $B_{12}Au^-$  and **16** for  $B_{13}O^-$ ) and low-lying structures (**2** and **3** for  $B_{12}Au^-$ ; **17** and **18** for  $B_{13}O^-$ ) and their corresponding neutral structures (**13–15** and **28–30**) at the B3LYP/B, O/6-311G(d,p)/Au/Stuttgart\_rsc\_1997\_ecp+2f1g level. The lowest vibrational frequency ( $\nu_{\min}$ ) and relative energy ( $\Delta E$ ) are labeled under each structure. The relative energy at the single-point CCSD(T)//B3LYP/B, O/6-311G(d,p)/Au/Stuttgart\_rsc\_1997\_ecp+2f1g level is shown in square brackets for the anions. Note structure **14** is a first order saddle point.

Again we optimized three neutral  $B_{13}O$  structures, **28–30** in Fig. 3, corresponding to the top three anionic structures. The neutral global minimum (**28**) is similar to its anion (**16**). Structure **29** is  $\sim 3.6$  kcal mol $^{-1}$  above **28**, whereas isomer **30** is higher in energy by  $\sim 18$  kcal mol $^{-1}$ .

## 5. Comparison between experiment and theory

We first use the well-characterized  $B_{12}^-$  cluster<sup>6</sup> to benchmark the B3LYP/6-311G(d,p) method, which predicted the ground-state



VDE and second VDE for  $B_{12}^-$  as 2.16 and 4.14 eV, respectively. These VDEs compare well with the experimental data of  $2.26 \pm 0.04$ , and  $4.31 \pm 0.05$  eV, reported previously,<sup>6</sup> although the B3LYP method seems to underestimate the VDEs by 0.1–0.2 eV. Similar errors are anticipated for the  $B_{12}Au^-$  and  $B_{13}O^-$  clusters.

### 5.1. $B_{12}Au^-$ : the global minimum

Structure **1** ( $C_1$ ,  $^1A$ ) is the global minimum for  $B_{12}Au^-$  at both the B3LYP/B/6-311G(d,p)/Au/ Stuttgart\_rsc\_1997\_ecp+2f1g and single-point CCSD(T)//B3LYP/B/6-311G(d,p)/Au/Stuttgart\_rsc\_1997\_ecp+2f1g levels (Fig. 3). Its calculated VDEs and simulated PES spectrum are compared with experimental measurements in Table 1 and Fig. 4a, respectively, where the simulated PES spectrum was constructed by fitting the distribution of the calculated VDEs with unit-area Gaussian functions of 0.05 eV half-width and each doublet final state was assumed to have equal intensity. The calculated ground-state ADE/VDE (3.16/3.34 eV) at B3LYP are systematically lower than the experimental data (3.48/3.59 eV) by  $\sim 0.3$  eV, consistent with the benchmarks of B3LYP *via*  $B_{12}^-$ , as mentioned above.<sup>47,48</sup> The single-point CCSD(T) data, 3.24/3.40 eV, are slightly improved. The simulated PES pattern is in excellent agreement with the main experimental features (Fig. 4a). Thus, the main PES bands for  $B_{12}Au^-$  (X and A–E) can be assigned reliably to the global minimum of  $B_{12}Au^-$  (Table 1). The overall agreement between the theoretical results and the experimental PES data suggest that the energetics of single-point CCSD(T) calculations is probably quite accurate.

### 5.2. $B_{12}Au^-$ : the minor isomer

The observed weak features X' and A' of  $B_{12}Au^-$  (Fig. 1) are due to coexisting minor isomers. Our calculations yield two low-lying isomers **2** ( $C_s$ ,  $^1A'$ ) and **3** ( $C_s$ ,  $^1A'$ ), which are within  $\sim 0.5$  kcal mol $^{-1}$  of the global minimum at the single-point CCSD(T) level (Fig. 3). The simulated PES spectrum of isomer **2** (Fig. 4b) shows the first two predicted VDEs at 3.76 and 4.27 eV, where the band intensity for isomer **2** (as well as that for isomer **3**; Fig. 4c) was weighed roughly according to the experimental X'/X ratio. These predicted VDE values are in good agreement with the observed minor bands X' ( $\sim 4.0$  eV) and A' ( $\sim 4.4$  eV), considering the B3LYP errors of 0.1–0.3 eV. Again, the calculated VDE at single-point CCSD(T) level is 3.85 eV, in slightly better agreement with band X'.

Isomer **3** (Fig. 4c) predicts a ground-state VDE of 3.57 and 3.66 eV, respectively, at B3LYP and single-point CCSD(T) levels, which numerically match the experimental VDE for band X (3.59 eV). However, considering the above-mentioned errors of B3LYP, the simulated spectrum is subject to a similar overall shift to the blue in order to compare faithfully with experiment. Such corrections deteriorate the agreement between the experimental and simulated spectra. The simulated PES spectrum also fails to reproduce the broad experimental A/B bands. Furthermore, the simulation predicts only one transition in the 5.6–6.3 eV binding energy regime, in contrast to two well-resolved experimental bands (D and E). It is stressed that a “missing” PES band in the simulation is a clear indication of a “wrong” cluster structure. It may thus be concluded that the contribution of

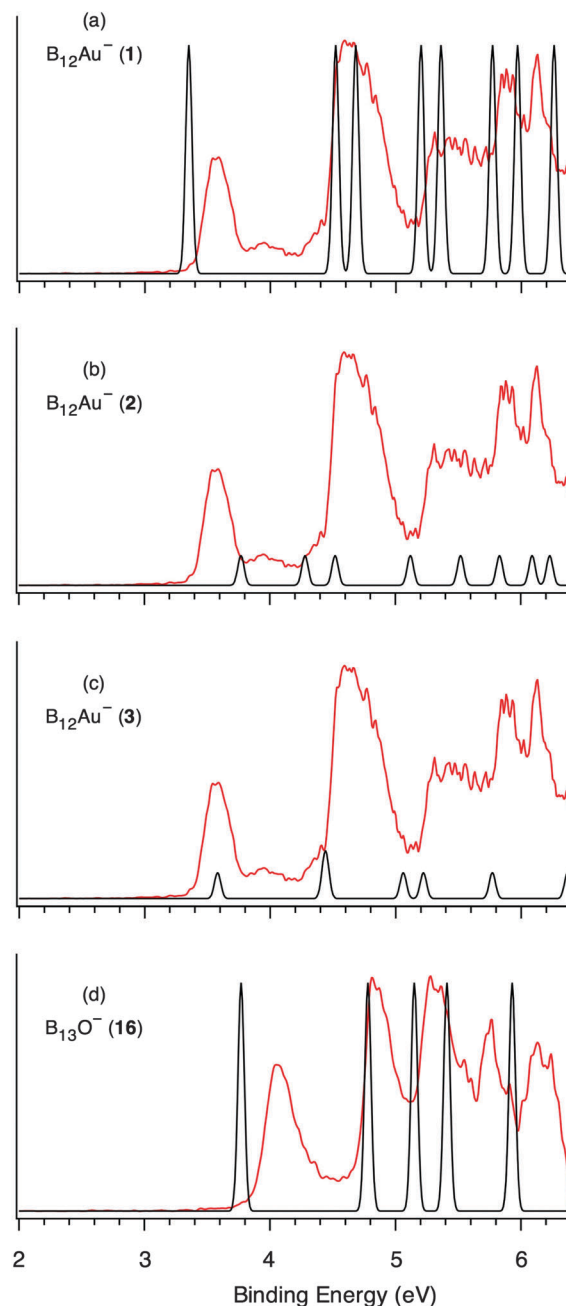


**Fig. 4** Simulated photoelectron spectra (black curves) at the B3LYP/B<sub>3</sub>O/6-311G(d,p)/Au/Stuttgart\_rsc\_1997\_ecp+2f1g level based on the global-minimum structures of (a)  $B_{12}Au^-$  (**1**) and (d)  $B_{13}O^-$  (**16**), as compared to the 193 nm experimental data (red curves). Low-lying isomers (b)  $B_{12}Au^-$  (**2**) and (c)  $B_{12}Au^-$  (**3**) are also included. The simulations were done by fitting the distribution of the calculated VDEs with unit-area Gaussian functions of 0.05 eV half-width. The band intensities for isomers **2** and **3** are weighed roughly to those of the minor experimental bands (X' and A') for better comparison.

isomer **3** is small, if any, and its corresponding PES features are likely to be buried below those from the main isomer **1**.

### 5.3. $B_{13}O^-$

The global minimum **16** ( $C_1$ ,  $^1A$ ) of  $B_{13}O^-$  is considerably more stable than the other low-lying isomers **17** ( $C_s$ ,  $^1A'$ ) and **18** ( $C_1$ ,  $^1A$ )

at the single-point CCSD(T)//B3LYP/6-311G(d,p) level, by 2.81 and 3.38 kcal mol<sup>-1</sup>, respectively. Indeed, in contrast to B<sub>12</sub>Au<sup>-</sup> (Fig. 1), no clear evidence is observed for any coexisting isomers for B<sub>13</sub>O<sup>-</sup> (Fig. 2). The calculated ground-state ADE/VDE (3.56/3.76 eV) at B3LYP/6-311G(d,p) compare well to the experimental values (3.90/4.04 eV), with the anticipated errors of ~0.3 eV. The simulated PES spectrum from the global minimum **16** displays peak-to-peak correspondence to the experimental data (Fig. 4d and Table 2). Isomers **17** and **18** can be ruled out on the basis of the energetics at the CCSD(T)//B3LYP/6-311G(d,p) level.

## 6. Discussion

### 6.1. Chemical bonding in B<sub>12</sub>Au<sup>-</sup> and B<sub>13</sub>O<sup>-</sup>

The above comparisons between experiment and theory establish the global-minimum structures of B<sub>12</sub>Au<sup>-</sup> (**1**) and B<sub>13</sub>O<sup>-</sup> (**16**) and their neutrals (**13** and **28**; Fig. 3). Basically, these structures are derived from the aromatic B<sub>12</sub><sup>-</sup> and B<sub>12</sub> clusters<sup>6</sup> and are similar to B<sub>12</sub>H<sup>-</sup> (**31**) and B<sub>12</sub>H (**43**) (Fig. S3 in ESI<sup>†</sup>). The simulated PES spectra based on **1**, **16**, and **31** are compared in Fig. S5 in the ESI<sup>†</sup>. The molecular orbitals of B<sub>12</sub>X<sup>-</sup> (X = Au, BO, H) are also compared with those of B<sub>12</sub><sup>-</sup> in the ESI<sup>†</sup> (Fig. S6–S8). Alternatively, chemical bonding in these systems can be understood from the adaptive natural density partitioning (AdNDP) analyses,<sup>49</sup> as shown in Fig. 5 for all three B<sub>12</sub>X<sup>-</sup> clusters. The X ligand is bonded to a peripheral B atom of B<sub>12</sub> *via* a 2c-2e σ bond, whereas the bonding elements of the B<sub>12</sub> motif are similar to bare B<sub>12</sub> cluster, that is, nine 2c-2e σ bonds for the B<sub>9</sub> peripheral ring, one 3c-2e σ bond for the inner B<sub>3</sub> triangle, five 3c-2e σ bonds for bonding between the inner triangle and the outer B<sub>9</sub> ring, and three delocalized π bonds. The H, Au, and BO ligands are all σ radicals, which form a single σ bond with B<sub>12</sub><sup>-</sup> using the extra electron, thus leaving the bonding in the B<sub>12</sub> motif intact. It is expected that additional ligands to the B<sub>12</sub> motif will start to break the B–B σ bonds on the peripheral B<sub>9</sub> ring, leading to instability of the B<sub>12</sub> motif and eventually to the anticipated 2D-to-cage structural transition.

### 6.2. Au–H isolobal analogy and boronyl chemistry

In recent years, we have found experimental and theoretical evidence that a single Au atom can act as H in alloy clusters such as the Si–Au and B–Au systems,<sup>23–25</sup> which is an extension of the isolobal analogy between a gold phosphine (AuPH<sub>3</sub>) unit and hydrogen in synthetic Au compounds.<sup>50</sup> The present results show that B<sub>12</sub>Au<sup>-</sup> and B<sub>12</sub>Au clusters are similar to B<sub>12</sub>H<sup>-</sup> and B<sub>12</sub>H clusters in terms of structures and bonding. This provides another example of the Au/H analogy, due to the high covalency of the B–Au bonding.<sup>51,52</sup> Indeed, natural bond orbital (NBO) analysis indicates little charge transfer within the Au–B bond: Q(Au) = -0.14 |e| and Q(B) = -0.29 |e| in B<sub>12</sub>Au<sup>-</sup> (**1**), and Q(Au) = +0.18 |e| and Q(B) = -0.17 |e| in B<sub>12</sub>Au (**13**). The B–Au bond distances are 2.10 Å in **1** and 2.05 Å in **13**, which are typical for a single bond.<sup>26</sup>

Our prior systematic studies on boron oxide clusters have uncovered the structural and chemical robustness of the boronyl BO group as a key structural unit, and also established the close

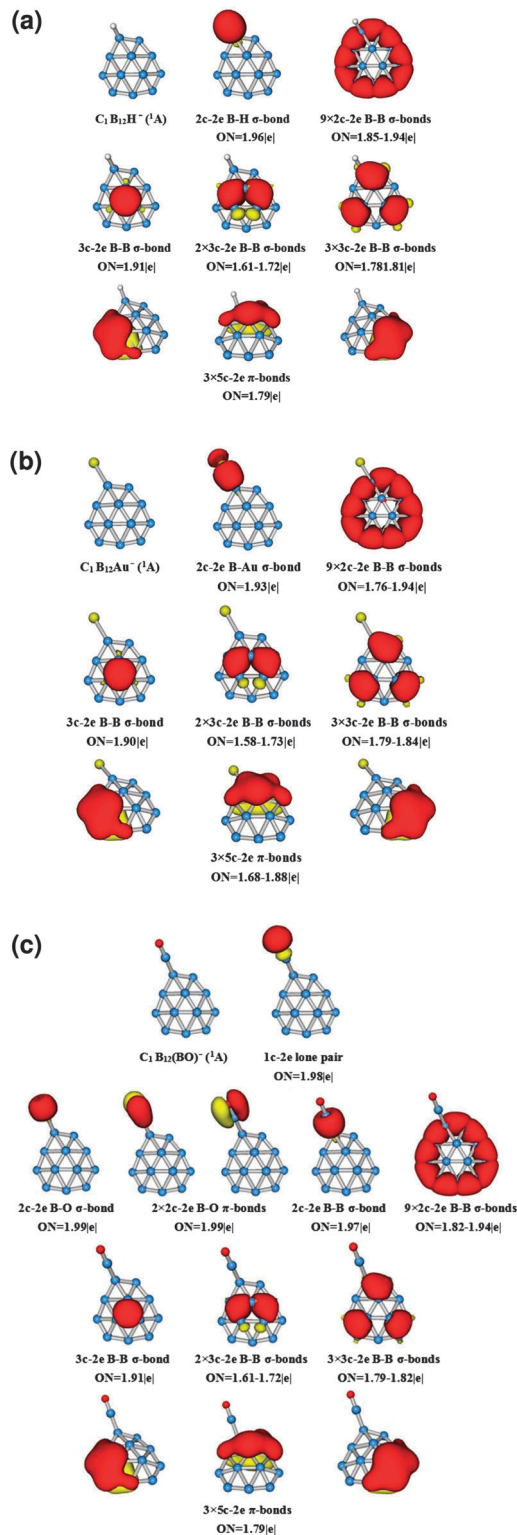


Fig. 5 AdNDP analyses for the chemical bonding in (a) B<sub>12</sub>H<sup>-</sup>, (b) B<sub>12</sub>Au<sup>-</sup>, and (c) B<sub>13</sub>O<sup>-</sup>.

analogy between boron-rich oxide clusters and boranes.<sup>27–30</sup> In the current B<sub>13</sub>O<sup>-</sup> (**16**) and B<sub>13</sub>O (**28**) clusters, the BO group again governs their structural and chemical properties. Note that **16** and **28** bear little structural resemblance to the B<sub>13</sub><sup>-</sup>, B<sub>13</sub>, or

$B_{13}^+$  clusters,<sup>3,4,6,13</sup> although the latter cation is a well-known “magic” cluster.<sup>14</sup> Importantly, the  $B\equiv O$  triple bond in the BO group is maintained in **16** and **28**, as reflected in their bond distances: 1.21 Å in **16** and 1.21 Å in **28**, which are compared to 1.203 and 1.234 Å in the gas-phase BO and  $BO^-$  clusters at the B3LYP/aug-cc-pVTZ level.<sup>27</sup> In addition, the B–B single bond associated with the BO group is also typical: 1.65 Å in **16** and 1.64 Å in **28**, as compared to those of 1.607 and 1.621 Å in  $B_4O_2^-$  and  $B_4O_2$  clusters at the B3LYP/aug-cc-pVTZ level.<sup>29</sup> Note that the B–( $B\equiv O$ ) single  $\sigma$  bond is also highly covalent, with an overall net charge of  $Q(B\equiv O) = +0.09 |e|$  in **16** and  $Q(B\equiv O) = +0.16 |e|$  in **28**.

## 7. Conclusions

In conclusion, we have studied the structural and electronic properties of the  $B_{12}Au^-$  and  $B_{13}O^-$  clusters and their neutral species using anion photoelectron spectroscopy and quantum chemical calculations. The electron affinities of  $B_{12}Au$  and  $B_{13}O$  are determined to be  $3.48 \pm 0.04$  and  $3.90 \pm 0.04$  eV, respectively. Two isomeric species are observed for  $B_{12}Au^-$ , whereas only one isomer for  $B_{13}O^-$  is observed. The global-minimum structures are found to consist of an intact  $B_{12}$  motif with the Au or BO ligand bonded to the periphery of the highly stable aromatic  $B_{12}$  cluster. Structures and bonding of  $B_{12}Au^-$  and  $B_{13}O^-$  are also found to be similar to the  $B_{12}H^-$  monohydride cluster. Thus, all three clusters are isolobal to each other and represent the first chemical compounds formed by the highly stable aromatic planar  $B_{12}$  cluster.

## Acknowledgements

S.D.L. would like to thank Professor A. I. Boldyrev for the Coalescence Kick (CK) global minimum search and the adaptive natural density partitioning (AdNDP) programs. This work was supported by the US National Science Foundation (DMR-0904034 to L.S.W.) and the National Natural Science Foundation of China (No. 20873117 to S.D.L.).

## Notes and references

- I. Boustani, *Int. J. Quantum Chem.*, 1994, **52**, 1081; I. Boustani, *Phys. Rev. B: Condens. Matter*, 1997, **55**, 16426.
- H. Kato, K. Yamashita and K. Morokuma, *Chem. Phys. Lett.*, 1992, **190**, 361; J. M. L. Martin, J. P. Francois and R. Gijbels, *Chem. Phys. Lett.*, 1992, **189**, 529; R. Kawai and J. H. Weare, *Chem. Phys. Lett.*, 1992, **191**, 311; A. Ricca and C. W. Bauschlicher, Jr., *Chem. Phys.*, 1996, **208**, 233; F. L. Gu, X. M. Yang, A. C. Tang, H. J. Jiao and P. v. R. Schleyer, *J. Comput. Chem.*, 1998, **19**, 203; J. I. Aihara, H. Kanno and T. Ishida, *J. Am. Chem. Soc.*, 2005, **127**, 13324; J. O. C. Jiménez-Halla, R. Islas, T. Heine and G. Merino, *Angew. Chem., Int. Ed.*, 2010, **49**, 5668.
- J. E. Fowler and J. M. Ugalde, *J. Phys. Chem. A*, 2000, **104**, 397.
- J. I. Aihara, *J. Phys. Chem. A*, 2001, **105**, 5486.
- B. Kiran, G. G. Kumar, M. T. Nguyen, A. K. Kandalam and P. Jena, *Inorg. Chem.*, 2009, **48**, 9965.
- H. J. Zhai, B. Kiran, J. Li and L. S. Wang, *Nat. Mater.*, 2003, **2**, 827.
- H. J. Zhai, A. N. Alexandrova, K. A. Birch, A. I. Boldyrev and L. S. Wang, *Angew. Chem., Int. Ed.*, 2003, **42**, 6004; A. N. Alexandrova, H. J. Zhai, L. S. Wang and A. I. Boldyrev, *Inorg. Chem.*, 2004, **43**, 3552.
- A. P. Sergeeva, B. B. Averkiev, H. J. Zhai, A. I. Boldyrev and L. S. Wang, *J. Chem. Phys.*, 2011, **134**, 224304.
- H. J. Zhai, L. S. Wang, A. N. Alexandrova and A. I. Boldyrev, *J. Chem. Phys.*, 2002, **117**, 7917; H. J. Zhai, L. S. Wang, A. N. Alexandrova, A. I. Boldyrev and V. G. Zakrzewski, *J. Phys. Chem. A*, 2003, **107**, 9319; A. N. Alexandrova, A. I. Boldyrev, H. J. Zhai, L. S. Wang, E. Steiner and P. W. Fowler, *J. Phys. Chem. A*, 2003, **107**, 1359; A. N. Alexandrova, A. I. Boldyrev, H. J. Zhai and L. S. Wang, *J. Phys. Chem. A*, 2004, **108**, 3509; A. P. Sergeeva, D. Yu. Zubarev, H. J. Zhai, A. I. Boldyrev and L. S. Wang, *J. Am. Chem. Soc.*, 2008, **130**, 7244; W. Huang, A. P. Sergeeva, H. J. Zhai, B. B. Averkiev, L. S. Wang and A. I. Boldyrev, *Nat. Chem.*, 2010, **2**, 202; Z. A. Piazza, W. L. Li, C. Romanescu, A. P. Sergeeva, L. S. Wang and A. I. Boldyrev, *J. Chem. Phys.*, 2012, **136**, 104310; A. P. Sergeeva, Z. A. Piazza, C. Romanescu, W. L. Li, A. I. Boldyrev and L. S. Wang, *J. Am. Chem. Soc.*, 2012, **134**, 18065.
- B. Kiran, S. Bulusu, H. J. Zhai, S. Yoo, X. C. Zeng and L. S. Wang, *Proc. Natl. Acad. Sci. U. S. A.*, 2005, **102**, 961.
- A. N. Alexandrova, A. I. Boldyrev, H. J. Zhai and L. S. Wang, *Coord. Chem. Rev.*, 2006, **250**, 2811.
- D. Yu. Zubarev and A. I. Boldyrev, *J. Comput. Chem.*, 2007, **28**, 251.
- E. Oger, N. R. M. Crawford, R. Kelting, P. Weis, M. M. Kappes and R. Ahlrichs, *Angew. Chem., Int. Ed.*, 2007, **46**, 8503.
- L. Hanley, J. L. Whitten and S. L. Anderson, *J. Phys. Chem.*, 1988, **92**, 5803; P. A. Hintz, S. A. Ruatta and S. L. Anderson, *J. Chem. Phys.*, 1990, **92**, 292; S. A. Ruatta, P. A. Hintz and S. L. Anderson, *J. Chem. Phys.*, 1991, **94**, 2833; M. B. Sowa-Resat, J. Smolanoff, A. Lapiki and S. L. Anderson, *J. Chem. Phys.*, 1997, **106**, 9511.
- S. Erhardt, G. Frenking, Z. F. Chen and P. v. R. Schleyer, *Angew. Chem., Int. Ed.*, 2005, **44**, 1078.
- C. Romanescu, A. P. Sergeeva, W. L. Li, A. I. Boldyrev and L. S. Wang, *J. Am. Chem. Soc.*, 2011, **133**, 8646.
- N. G. Szwacki, V. Weber and C. J. Tymczak, *Nanoscale Res. Lett.*, 2009, **4**, 1085; S. Sahu and A. Shukla, *Nanoscale Res. Lett.*, 2010, **5**, 714.
- G. Forte, A. La Magna, I. Deretzis and R. Pucci, *Nanoscale Res. Lett.*, 2010, **5**, 158.
- Y. Ohishi, K. Kimura, M. Yamaguchi, N. Uchida and T. Kanayama, *J. Phys.: Conf. Ser.*, 2009, **176**, 012030.
- H. Bai and S. D. Li, *J. Cluster Sci.*, 2011, **22**, 525.
- N. G. Szwacki and C. J. Tymczak, *Nanoscale Res. Lett.*, 2012, **7**, 236.
- Y. Ohishi, K. Kimura, M. Yamaguchi, N. Uchida and T. Kanayama, *J. Chem. Phys.*, 2008, **128**, 124304; Y. Ohishi, K. Kimura, M. Yamaguchi, N. Uchida and T. Kanayama, *J. Chem. Phys.*, 2010, **133**, 074305.
- H. J. Zhai, L. S. Wang, D. Yu. Zubarev and A. I. Boldyrev, *J. Phys. Chem. A*, 2006, **110**, 1689.



- 24 B. Kiran, X. Li, H. J. Zhai, L. F. Cui and L. S. Wang, *Angew. Chem., Int. Ed.*, 2004, **43**, 2125; X. Li, B. Kiran and L. S. Wang, *J. Phys. Chem. A*, 2005, **109**, 4366; B. Kiran, X. Li, H. J. Zhai and L. S. Wang, *J. Chem. Phys.*, 2006, **125**, 133204.
- 25 Q. Chen, H. J. Zhai, S. D. Li and L. S. Wang, *J. Chem. Phys.*, 2013, **138**, 084306.
- 26 D. Yu. Zubarev, J. Li, L. S. Wang and A. I. Boldyrev, *Inorg. Chem.*, 2006, **45**, 5269.
- 27 H. J. Zhai, L. M. Wang, S. D. Li and L. S. Wang, *J. Phys. Chem. A*, 2007, **111**, 1030.
- 28 H. J. Zhai, S. D. Li and L. S. Wang, *J. Am. Chem. Soc.*, 2007, **129**, 9254.
- 29 S. D. Li, H. J. Zhai and L. S. Wang, *J. Am. Chem. Soc.*, 2008, **130**, 2573.
- 30 D. Yu. Zubarev, A. I. Boldyrev, J. Li, H. J. Zhai and L. S. Wang, *J. Phys. Chem. A*, 2007, **111**, 1648; W. Z. Yao, J. C. Guo, H. G. Lu and S. D. Li, *J. Phys. Chem. A*, 2009, **113**, 2561; H. J. Zhai, C. Q. Miao, S. D. Li and L. S. Wang, *J. Phys. Chem. A*, 2010, **114**, 12155; H. J. Zhai, J. C. Guo, S. D. Li and L. S. Wang, *ChemPhysChem*, 2011, **12**, 2549; Q. Chen, H. J. Zhai, S. D. Li and L. S. Wang, *J. Chem. Phys.*, 2012, **137**, 044307.
- 31 A. N. Alexandrova, E. Koyle and A. I. Boldyrev, *J. Mol. Model.*, 2006, **12**, 569.
- 32 M. L. Drummond, V. Meunier and B. G. Sumpter, *J. Phys. Chem. A*, 2007, **111**, 6539; T. B. Tai and M. T. Nguyen, *Chem. Phys. Lett.*, 2009, **483**, 35; M. T. Nguyen, M. H. Matus, V. T. Ngan, D. J. Grant and D. A. Dixon, *J. Phys. Chem. A*, 2009, **113**, 4895; C. B. Shao, L. Jin, L. J. Fu and Y. H. Ding, *Mol. Phys.*, 2009, **107**, 2395; C. B. Shao, L. Jin, L. J. Fu and Y. H. Ding, *Theor. Chem. Acc.*, 2009, **124**, 161; T. B. Tai, M. T. Nguyen and D. A. Dixon, *J. Phys. Chem. A*, 2010, **114**, 2893; C. B. Shao, L. Jin and Y. H. Ding, *J. Comput. Chem.*, 2011, **32**, 771.
- 33 S. D. Li, C. Q. Miao, J. C. Guo and G. M. Ren, *J. Comput. Chem.*, 2005, **26**, 799; G. M. Ren, S. D. Li and C. Q. Miao, *THEOCHEM*, 2006, **770**, 193.
- 34 H. Braunschweig, K. Radacki and A. Schneider, *Science*, 2010, **328**, 345.
- 35 H. Braunschweig, R. D. Dewhurst, K. Hammond, J. Mies, K. Radacki and A. Vargas, *Science*, 2012, **336**, 1420.
- 36 L. S. Wang, H. S. Cheng and J. Fan, *J. Chem. Phys.*, 1995, **102**, 9480.
- 37 L. S. Wang and X. Li, in *Clusters and Nanostructure Interfaces*, ed. P. Jena, S. N. Khanna and B. K. Rao, World Scientific, New Jersey, 2000, pp. 293–300.
- 38 A. D. Becke, *J. Chem. Phys.*, 1993, **98**, 5648; C. Lee, W. Yang and R. G. Parr, *Phys. Rev. B*, 1988, **37**, 785.
- 39 J. S. Binkley, J. A. Pople and W. J. Hehre, *J. Am. Chem. Soc.*, 1980, **102**, 939.
- 40 M. Saunders, *J. Comput. Chem.*, 2004, **25**, 621; P. P. Bera, K. W. Sattelmeyer, M. Saunders and P. v. R. Schleyer, *J. Phys. Chem. A*, 2006, **110**, 4287.
- 41 R. Krishnan, J. S. Binkley, R. Seeger and J. A. Pople, *J. Chem. Phys.*, 1980, **72**, 650.
- 42 J. M. L. Martin and A. Sundermann, *J. Chem. Phys.*, 2001, **114**, 3408.
- 43 M. E. Casida, C. Jamorski, K. C. Casida and D. R. Salahub, *J. Chem. Phys.*, 1998, **108**, 4439; R. Bauernschmitt and R. Ahlrichs, *Chem. Phys. Lett.*, 1996, **256**, 454.
- 44 J. Cizek, *Adv. Chem. Phys.*, 1969, **14**, 35; G. E. Scuseria and H. F. Schaefer, *J. Chem. Phys.*, 1989, **90**, 3700; R. J. Bartlett and M. Musial, *Rev. Mod. Phys.*, 2007, **79**, 291.
- 45 M. J. Frisch, *et al.*, Gaussian 03, revision A.1, Gaussian, Inc., Pittsburgh, PA, 2003.
- 46 H. J. Zhai and L. S. Wang, *J. Chem. Phys.*, 2005, **122**, 051101; H. J. Zhai, B. Kiran, B. Dai, J. Li and L. S. Wang, *J. Am. Chem. Soc.*, 2005, **127**, 12098; H. J. Zhai, L. L. Pan, B. Dai, B. Kiran, J. Li and L. S. Wang, *J. Phys. Chem. C*, 2008, **112**, 11920; Y. L. Wang, H. J. Zhai, L. Xu, J. Li and L. S. Wang, *J. Phys. Chem. A*, 2010, **114**, 1247.
- 47 Zero-point energies (ZPEs) are not included in the B3LYP/B, O/6-311G(d,p)/Au/Stuttgart\_rsc\_1997\_ecp+2f1g data listed in Tables 1 and 2. With ZPE corrections, the ground-state ADEs are 3.15 eV for B<sub>12</sub>Au<sup>−</sup> (**1**) and 3.54 eV for B<sub>13</sub>O<sup>−</sup> (**16**), which are within 0.01–0.02 eV of the original data.
- 48 Considering that the basis sets may be inadequate in dealing with anions because they do not include diffuse functions, we have run additional B3LYP calculations using the 6-311++G(d,p) basis sets for B and O. The calculated ground-state ADEs/VDEs are 3.19/3.37 eV for B<sub>12</sub>Au<sup>−</sup> (**1**) and 3.64/3.84 eV for B<sub>13</sub>O<sup>−</sup> (**16**), which are in slightly better agreement with experiment. But the improvement is only 0.03 eV for B<sub>12</sub>Au<sup>−</sup> and 0.08 eV for B<sub>13</sub>O<sup>−</sup>.
- 49 D. Yu. Zubarev and A. I. Boldyrev, *Phys. Chem. Chem. Phys.*, 2008, **10**, 5207.
- 50 For selected reviews, see: K. P. Hall and D. M. P. Mingos, *Prog. Inorg. Chem.*, 1984, **32**, 237; P. G. Jones, *Gold Bull.*, 1981, **14**, 102; 1981, **14**, 159; 1983, **16**, 114; 1986, **19**, 46.
- 51 L. S. Wang, *Phys. Chem. Chem. Phys.*, 2010, **12**, 8694.
- 52 C. Q. Miao, H. G. Lu and S. D. Li, *J. Cluster Sci.*, 2013, **24**, 233.